

Direct localisation of molecules in tissue sections of growing antler tips using MALDI imaging

Santanu Deb-Choudhury $^1\cdot$ Wenying Wang $^2\cdot$ Stefan Clerens $^1\cdot$ Chris McMahon $^3\cdot$ Jolon M. Dyer $^1\cdot$ Chunyi Li 2,4

Received: 4 June 2015 / Accepted: 6 August 2015 © Springer Science+Business Media New York 2015

Abstract The astonishing growth rate of deer antlers offers a valuable model for the discovery of novel factors and regulatory systems controlling rapid tissue growth. Numerous molecules have been identified in growing antlers using a variety of techniques. However, little is known about the spatial distribution of these molecules in situ. A technique that has the potential to help in this regard is direct proteomic analysis of tissue sections by matrix-assisted laser desorption/ionization imaging mass spectrometry (MALDI-IMS). The present study applied this technique to spatially map molecules in antler tissue sections. Two protonated molecular ions were selected: m/z 6679 and m/z 6200 corresponding to VEGF and thymosin beta-10, respectively. Superimposition of the respective ion images on to histologically stained samples showed distinct spatial distribution across the antler tissue sections which were consistent with the previous reports using in situ hybridization. Two other molecular ions specifically m/z 8100 and m/z 11,800 were also selected, corresponding to reported masses of urocortin precursor and thioredoxin, respectively. As the spatial distribution of these proteins is not specifically known, MALDI-IMS was used as a potential technique to obtain information on their distribution on antler tips. The presence of all these molecules in deer antlers were further confirmed using LC–MS/MS data. The present study also demonstrated that MALDI-IMS could be further used to image antler sections with an extended ion mass range of up to m/z 45,000, thus potentially increasing the ability to discover the distribution of a larger set of molecules that may play an important role in antler growth. We have thus demonstrated that MALDI-IMS is a promising technique for generating molecular maps with high spatial resolution which can aid in evaluating the function of novel molecules during antler growth.

Keywords Deer · Antler · MALDI-IMS · Growth centre · Proliferation

Introduction

Deer antlers are unique mammalian appendages in that once lost they can fully regenerate. Therefore, they offer an excellent opportunity to investigate mechanisms underlying regeneration of mammalian organ [1]. Antlers regenerate in yearly cycles: casting off previous hard antlers and initiation of new soft antlers in spring, rapid antler growth and maturation in summer, full antler calcification and antler skin shedding in autumn, and the bare bony antler phase in winter [2–4]. During the growth phase, elongation of antlers can exceed 2 cm a day [5], which is arguably the fastest growing tissue in mammals. Surprisingly, under such an unprecedented rate of growth, antlers always form well-organised structure and do not become

Published online: 11 August 2015



Santanu Deb-Choudhury santanu.deb-choudhury@agresearch.co.nz

[☐] Chunyi Li lichunyi1959@163.com

AgResearch, Food & Bio-Based Products, Lincoln Research Centre, Christchurch, New Zealand

² AgResearch Invermay Agricultural Centre, 50034, Mosgiel, New Zealand

³ AgResearch Ruakura Agricultural Centre, 3123, Hamilton, New Zealand

State Key Laboratory for Molecular Biology of Special Economic Animals, 4899 Juye Street, Changchun Jilin, People's Republic of China

tumourigenic. Therefore, the mechanisms underlying antler growth may be invaluable for identifying factors that can regulate the rapid and co-ordinated regeneration of organs without the detrimental effects of tumourigenesis [6, 7].

It is known that the antler growth centre is located at the antler tip, which was initially demonstrated by insertion of a nail in the middle of a growing antler. Eleven days after inserting the nail, the distance between the nail and the antler tip increased from 3.5 to 5.5 cm, while the distance between the nail and the antler base remained unchanged [8]. The histological makeup of antler tips has been extensively investigated in the last century, and Banks and Newbery [9] classified an antler growth centre into four zones. These are distoproximally proliferation, maturation, hypertrophy, and calcification zones. The proliferation zone includes three layers: reserve mesenchyme (RM), precartilage, and cartilage. This classification was subsequently adopted by other studies [10–13].

The incorporation of BrdU (Bromodeoxyuridine) used for detecting proliferating cells in vivo has been invaluable in confirming the histological findings and to pinpoint the cell types responsible for rapid growth of antlers. Those studies revealed that the majority of proliferating cells in an antler tip are concentrated in the inner sublayer of the RM, whereas the outer sublayer of the RM is almost devoid of BrdU-labelled cells [14, 15]. Based on the histological results, BrdU incorporation findings and morphologically identifiable markers, the classification for the antler proliferation zone from Banks and Newbery [9] was further refined into a distoproximally layer of RM including outer and inner sublayers, layer of precartilage, layer of transition, and layer of cartilage [14, 16]. Due to the practicality of this classification for sampling fresh antler tissues, it has been widely used for the identification of novel factors from cDNA libraries [14, 17-20], microarray analyses [21, 22], or proteomic approaches [23–25]. While those studies have made a great contribution to the identification of molecules that regulate the growth of antlers, they offered little or no information about the spatial distribution of molecules, or the intensity of expression within the tissue. This is because localisation and the identification of molecules within tissue sections through the classical techniques present formidable tasks. This situation has hampered progress in ascribing biological functions to the identified molecules in the antler system.

The direct proteomic analysis of tissue sections by matrix-assisted laser desorption/ionization imaging mass spectrometry (MALDI-IMS) is well established. This technique can be performed on intact tissue for the determination of the spatial distribution of the molecules and their relative expression levels without the need to use radio-labelled probes (in situ hybridization) or immunochemical reagents. The MALDI-IMS technique has been

successfully used as a discovery oriented tool for non-targeted investigations. This technique is particularly suitable for localising the spatial distribution and expression of a wide range of endogenous compounds such as proteins, peptides, and lipids [26–30].

The aim of this study was to test the suitability of the MALDI-IMS technique on antler tissue samples by directly localising some of the selected molecules involved in antler growth and consecutively confirming their identity using gel-enhanced liquid chromatography-mass spectrometry (GeLC-MS). Knowledge of the spatial distribution of these molecules in the antler growth centre would thus help in elucidating a possible role in antler growth.

Materials and methods

Materials

Ammonium bicarbonate, CHAPS, dichloromethane, ethanol, isopropanol, acetone, guanidine, methanol, potassium hydroxide, Tris, and urea were obtained from Merck (Darmstadt, Germany). Formic acid (FA) and TFA were from BDH (Poole, Dorset, England). TPCK-trypsin was obtained from Promega Corporation (Madison, WI, USA). Tris(2-carboxyethyl) phosphine (TCEP) was obtained from Fluka Chemie GmbH (Buchs, Germany). Sinnapinic acid (SA) (D-7927) was from Sigma. Indium-tin oxide (ITO) coated MALDI target slides and α -Cyano-4-hydroxy-cinnamic acid (HCCA) were from Bruker Daltonik (Bremen, Germany).

Antler tissue sampling

Three sticks of growing antlers were used for this study. The first was an antler harvested at the incipient stage (5 cm long on the top of a full grown pedicle from a 9-month-old red deer stag), which was collected from a slaughter plant (Otago Venison) immediately after slaughter. The second and the third were growing antlers extended to 60 days post casting from two 3-year-old red deer stags on two occasions (one antler/deer/occasion). The antler removal procedure was in accordance with regulations set by the New Zealand National Velveting Standard Board. The distal 3 cm of the tip from each antler was cut off and sectioned sagittally along the longitudinal axis. The tip was then cut into 5-mm-thick slices along the same plane. The slices were further cut into strips 1-2 cm across (for further details see [16]. To include the full width of all the tissue layers in an antler growth centre, only the strips from the central regions were collected. The central pieces were quickly frozen on dry ice and then stored at -80 °C.



Tissue preparation

Frozen antler samples were quickly transferred to a freezing microtome chamber (Leica CM 1850; Leica Microsystems, Germany) that was maintained at -20 °C. The samples were mounted onto cryostat specimen stubs with a minimal amount of optimal cutting temperature (OCT) mounting medium (Jung tissue freezing medium, Leica Instruments, Germany) ensuring that OCT was not present on the tissue sections. OCT is known to suppress the formation of ions and interfere with MALDI-IMS [31]. The samples were allowed to equilibrate at -20 °C before sectioning inside the cryostat chamber. Sections were cut at 15 µm thickness and mounted onto ITO slides. Liquid whiteout was used to mark the corners of the sections to serve as reference points to help align the images. A native image was then obtained using a low resolution (1500 dpi) scan.

To correlate the MS data obtained through MALDI-IMS with the histological features of the same tissue section, a sequential wash with 100 % methanol for 10 min followed by 100 % acetone wash for 5 min was used to remove the matrix and fix the tissue prior to staining. The sections were then air dried and counter-stained using haematoxylin and eosin/alcian blue [12].

Sample preparation for proteins below 20 kDa for MALDI-IMS

Tissue sections placed on the ITO-coated slides were sequentially fixed with 70 % ethanol followed by 90 % ethanol to eliminate the presence of most phospholipids and physiological salts. The sections were then dried in a desiccator prior to MALDI matrix application. Matrix solution consisting of 10 g/L SA in 60 % acetoniotrile (0.2 % TFA) was evenly sprayed onto the surface of the sample section using an ImagePrep device (Bruker) with the standard SA method provided with the instrument. In order to reduce the likelihood of lateral gradient formations during application of the matrix, the spraying, incubation and drying times were properly controlled.

MALDI images were acquired using a Bruker Ultraflex III TOF/TOF using FlexImaging 2.1 (Bruker) in linear positive ion mode in a mass range of 2000–20,000 Da with a sampling rate of 0.1 gigasamples/s. Acquisition was performed using a Smart beam laser with a repetition rate of 200 Hz. A spatial resolution of either 100 or 200 μ m was used and each MS spectrum was obtained upon accumulation of 400 consecutive laser shots. Images were reconstructed using Fleximaging 2.0 and normalised using a 0.5 $Y_{\rm mean}/Y_{\rm max}$ threshold.

External calibration of the spectra was performed using a Protein Calibration Standard (Bruker) diluted threefold

with matrix solution, which was spotted on one corner of the section.

Sample preparation for proteins above 20 kDa for MALDI-IMS

Some previously identified molecules from growing antler tips were found to be above 20 kDa [23] and to include them in MALDI-IMS, required a modified method. To increase the mass range of proteins that could be detected using MALDI-IMS, the sandwich technique was used [32]. This technique involved co-crystallisation of the matrix with the analyte. A drop of SA matrix at a concentration of 20 mg/mL in 90 % ethanol, 0.1 % trifluoroacetic acid (TFA), and 0.5 % Triton X-100 was placed on a ITO-coated slide and a tissue section positioned on it. The matrix was then allowed to dry and a seed layer of SA crystals dispersed in xylene was then added on the tissue section. An additional layer of SA in 90 % ethanol containing 0.1 % TFA was applied. This was then followed by a final layer of SA in 50 % ACN and 0.1 % TFA.

External calibration of the spectra was performed using a Protein Calibration Standard as described above.

GeLCMS

A routine bottom-up proteomic analysis was adopted to identify proteins from the tryptic digests of antler tip shavings using LC-MS/MS, to confirm whether the molecular masses visualised by MALDI-IMS truly relate to proteins in the antler tissue. Deer antler shavings were solubilised using 7 M urea, 2 M thiourea, 4 % CHAPS, 50 mM DTT, and 2 % Pharmalyte pH 3-10 (v/v). Fifteen µl of the extract was separated on a 4-20 % T SDS-PAGE gel and stained with Blue Silver stain.

Six bands were excised, evenly spaced, from the region of the gel with proteins 20 kDa and below. The gel slices were then reduced with TCEP followed by alkylation with acrylamide, after which they were digested using 2 μg TPCK-trypsin in 10 % ACN, 50 mM ammonium bicarbonate for 18 h at 37 °C. The supernatants were collected first, followed by further extraction of peptides from the gels by vortexing for 10 min in 50 mM ammonium bicarbonate, 50 % ACN, 0.5 % FA or 0.1 % TFA, and then in 80 % ACN. The fractions were pooled and concentrated using a vacuum centrifugal concentrator (Labconco, Kansas City, MI, USA). The digests were subsequently analysed using LC–MS/MS.

LC-MS/MS

Nanoflow LC-MS/MS was performed on an LC-Packings (Amsterdam, Holland) system, consisting of a Famos



autosampler, a Switchos column-switching module, and an Ultimate nanoflow pump. Ten µL samples were loaded on an in-house packed pre-column (Varian MicroSorb C18, 20 cm, 75 μm ID, 300 Å pore size, 5 μm particles) at a flow rate of 8 µl/min. The pre-column was then switched in-line with an in-house packed analytical column with the same sorbent as that of the pre-column. The reversed-phase elution gradient ran from 5 to 70 % ACN (including 0.2 % FA) in 45 min, at 150 nl/min. The column outlet was directly connected to a QSTAR Pulsar i (ABSciex, Foster City, CA, USA) using a Proxeon stainless steel electrospray needle. The OSTAR software was programmed for automatic acquisition of MS-TOF (MS-Time Of Flight) survey spectra, followed by MS/MS-TOF fragmentation of detected $[M + H]^+$, $[M + 2H]^{2+}$ and $[M + 3H]^{3+}$ peaks. MS data were acquired from m/z (mass to charge value) 400-1200 and MS/MS from m/z 40-1600 accumulating three cycles, each with 1.3 s duration.

Data analysis

After the LC-MS/MS run, the Mascot script for Analyst QS 1.1 (Matrix Science, London, UK) was used to extract peak lists from the data. The peak lists were searched against the NCBInr database (date: 11th March 2009) using an inhouse Mascot server (Mascot v2.2.06, Matrix Science). Enzyme specificity was set to semi-trypsin and taxonomy restricted to Bovidae, in the search criteria. Propionamide was specified as a fixed modification and methionine oxidation as a variable modification. Two missed cleavages were allowed and the error tolerance was 0.2 Da for both LC ESI-MS and MS/MS. ProteinScape 2.1 (Bruker) was used to store peak list data and result analysis. Acceptance thresholds for peptide and protein scores were set at 20 and 50, respectively, with at least one significant peptide identity score calculated by the search engine required for protein identification. Protein lists were compiled using the Protein Extractor function and only those results assessed as true matches were used for further analysis.

Results and discussion

Histological makeup of the antler growth centre

Based on staining with haemotoxylin and eosin/alcian blue, each growing antler tip at the time of sampling was determined to clearly consist of six layers: distoproximally dermis, vascular, reserve mesenchyme, precartilage, transition, and cartilage layers. Compared to the layers of the first antler (Fig. 1a), antlers at 60 days growth had wider dermal, reserve mesenchyme, precartilage, and cartilage layers but had a narrower vascular layer and a similar

transition layer (Fig. 1b). The reserve mesenchyme could be divided into two sublayers: outer (pinkish, ORM) and inner (bluish, IRM) sublayers. The precartilage region was evident by the discrete vascular channels and the less mature chondroblasts (the least stained region, precartilage). The cartilage layer featured continuous vascular channels and dark blue staining. Between the precartilage layer and the cartilage layer, a transition layer was located, within which discrete channels gradually merged into continuous vascular channels.

LC-MS/MS approach

Over 40 different proteins were identified from the antler tissue using a routine LC-MS/MS approach (Table 1). The ion masses obtained from the MALDI-IMS, described below, were then correlated with the identified proteins from the LC-MS/MS study.

Use of MALDI-IMS technique for antler tissue studies

Spatial distribution of the corresponding masses of proteins, identified using LC-MS/MS, was determined from ion images obtained using MALDI-IMS. Following MALDI-IMS, the acquired ion images were superimposed onto the histological sections of antler tips to correlate the spatial distribution of the selected proteins with different layers and cell types. A routine MALDI-IMS approach was undertaken to visualise the spatial distribution of proteins in the mass range m/z 2000 to 20,000. The global mass spectrum acquired in the positive ion mode from m/z 4000 to 20,000 is shown in Fig. 2a. Although most of the ions with high intensities were seen in the lower end of the scale restricted below m/z 7000, a number of good signal intensities were obtained up to m/z16,000.

Selection of specific molecular ions on tissue sections

Two protonated molecular ions, specifically m/z 8100 (red bar) and 11,800 (green bar) were selected as these ions possibly correspond to the reported masses of urocortin precursor and thioredoxin, respectively (Fig. 2a). Both these proteins were considered to be present in the antler tissue as determined from the LC-MS/MS study (Table 1). In order to determine their spatial distribution on antler tips, superimposition of the ion images onto the corresponding histological sections visually revealed a higher ion intensity of m/z 8100 (urocortin precursor) in the vascular layer, precartilage layer and the transition layer compared to the rest of the layers of the antler tip (Fig. 2b). However, the distribution of m/z 11,800 (thioredoxin)



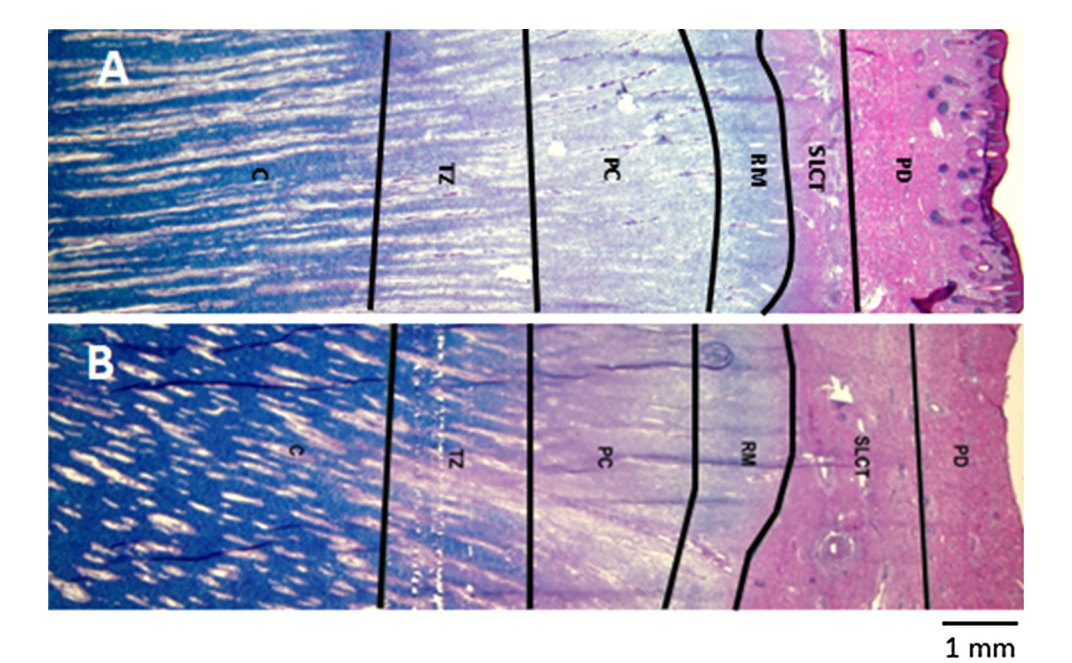


Fig. 1 Histological sections of growing red deer antler tips counterstained with haematoxylin and eosin, and alcian blue. These sections clearly consisted of 6 layers distoproximally dermal (PD), vascular

(SLCT), reserve mesenchymal (RM), precartilage (PC), transitional (TZ), and cartilage (C). **a** Antler tip section from a 9-month-old stag calf. **b** Antler tip section from a 3-year-old stag

appeared to be evenly distributed throughout the antler tip (Fig. 2c).

Urocortin belongs to the corticotropin-releasing factor (CRF)/urotensin I family and plays biologically diverse roles in several systems such as cardiovascular, reproductive, stress, and inflammatory responses. In the cardiovascular system, urocortin has potent local vasodilatory effects [33, 34]. Bale et al. [35] reported that urocortin 2 can effectively suppress angiogenesis through binding to CRF receptor 2. In the present study, a slightly higher intensity of the molecular ion m/z 8100 (urocortin precursor) in the vascular layer of antler tips indicates that this molecule may play a role in relaxation of blood vessels in order to cope with the high metabolic demand during rapid antler growth [9]. In contrast, urocortin may have a role in counter-balancing of vascular endothelial growth factor (VEGF) function for controlling vascular system formation in the precartilage layer and transition layer, because VEGF is also expressed in these regions [36] and urocortin inhibits angiogenesis [35].

Thioredoxin is an oxidative stress-inducible biological antioxidant in mammalian cells and reduces its target proteins using highly conserved thiol groups [37]. Therefore, thioredoxin is very important for protecting cells from the detrimental effects of reactive oxygen species. During each spring and summer, antler growth can reach 2 cm/day [5], arguably the fastest growing tissue in mammals. This growth rate undoubtedly produces a high abundance of reactive oxygen species in every cell type of the whole

antler growth centre, which could account for the presence of the molecular ion m/z 11,800 possibly corresponding to thioredoxin, throughout the antler growth regions.

Molecules known to be expressed in antler tissue

Two molecules namely VEGF and thymosin beta-10 known to be expressed in antler tip tissue were selected for validation of the MALDI-IMS approach. Antler tip section from 3-year-old deer was chosen for validation because these two molecules were previously localised using in situ hybridization on antler sections from 3-year [36, 42]. The molecular masses of these two proteins correspond to m/z 6679 and 6200, respectively, in the ion spectrum (Figs. 3a, c). The ion images superimposed on the histological sections of antler tips for VEGF (Fig. 3b) and thymosin beta-10 (Fig. 3d), respectively, revealed that both of these proteins were mainly concentrated in the transition and in the precartilage layer, with nearly negligible amounts present in the cartilage layer. However, VEGF protein had very little and thymosin beta-10 had an appreciable presence in the vascular layer and in the dermis.

VEGF is a homodimeric glycoprotein, which plays a major role in stimulating vasculogenesis and angiogenesis [38, 39]. While studying angiogenesis in growing antlers, Clark et al. [36] found that VEGF mRNA was mainly localised in the precartilage region, but was not found in the vascular layer, which is consistent with the findings in the present study. Furthermore, these authors [36] reported



Table 1 Peptide sequences of proteins and their corresponding masses identified using LC-MS/MS from deer antler

1 1 1))				
Protein name/accession number	MW (kDa)	m/z meas.	Z	Score	Range	Sequence	Modification
Histone H4 gil27806945	7.6	442.5895	3	30.2	8–19	R.DNIQGITKPAIR.R	
		548.8314	2	41.9	10–19	N.IQGITKPAIR.R	
		492.2892	2	49.1	11–19	I.QGITKPAIR.R	
		590.8038	2	62.8	30–39	R.ISGLIYEETR.G	
		495.2831	2	46.1	44–51	K.VFLENVIR.D	
		567.7743	2	34.4	52–61	R.DAVTYTEHAK.R	
		474.7418	2	42.8	54–61	A.VTYTEHAK.R	
		425.2030	2	30.6	55-61	V.TYTEHAK.R	
		655.8406	2	65.7	64–75	K.TVTAMDVVYALK.R	
		663.8419	2	82.4	64–75	K.TVTAMDVVYALK.R	Oxidation: 5
Chain P, the structure of crystalline	14.9	607.3114	2	48.1	26–37	K.DSPSVWAAVPGK.T	
profilin-beta-actin gil576369		829.4615	2	37.5	38–53	K.TFVNITPAEVGILVGK.D	
		727.8766	2	55.9	69–95	R.SSFFVNGLTLGGQK.C	
		828.3701	2	87.4	75–88	R.DSLLQDGEFTMDLR.T	Oxidation: 11
		820.3647	2	100.1	75–88	R.DSLLQDGEFTMDLR.T	
		856.9211	2	46.8	91–107	K.STGGAPTFNITVTMTAK.T	Oxidation: 14
		437.7608	2	23.0	108-115	K.TLVLLMGK.E	
		445.7712	2	34.0	108-115	K.TLVLLMGK.E	Oxidation: 6
Histone cluster 2, H2bf gil66912162	13.9	569.2737	2	32.5	36–44	K.ESYSVYVYK.V	
		584.7908	2	28.0	48–58	K.QVHPDTGISSK.A	
		413.8852	3	40.8	48–59	K.QVHPDTGISSKA.M	
		888.4000	2	96.4	59–73	K.AMGIMNSFVNDIFER.I	Oxidation: 2, 5
		620.7955	2	58.5	64–73	M.NSFVNDIFER.I	
		477.3029	2	56.0	101–109	R.LLLPGELAK.H	
		727.3952	-	28.1	103–109	L.LPGELAK.H	
		614.3306	_	22.5	104–109	L.PGELAK.H	
		414.7108	2	29.1	110-117	K.HAVSEGTK.A	
Hemoglobin subunit beta gil122569	16.0	475.7567	2	64.6	8–16	K.AAVTAFWGK.V	
		808.4028	-	20.6	10–16	A.VTAFWGK.V	
		637.8592	2	52.6	30–39	R.LLVVYPWTQR.F	
		633.3844	2	78.8	104–115	K.LLGNVLVVVLAR.H	
		604.3314	2	82.7	132-143	K.VVTGVANALAHR.Y	
		505.2678	2	78.5	134–143	V.TGVANALAHR.Y	
Albumin precursor gil193085052	66.3	478.5732	3	41.3	65–76	K.SLHTLFGDELCK.V	Propionamide: 11
		571.8493	2	35.5	524–533	K.KQTALVELLK.H	
		507.8090	2	59.8	525–533	K.QTALVELLK.H	
		729.0391	3	50.7	538–556	K.ATDEQLKTVMENFVAFVDK.C	
		708.3468	2	64.5	545–556	K.TVMENFVAFVDK.C	Oxidation: 3



Table 1 continued									
Protein name/accession number	MW (kDa)	m/z meas.	Z		S	Score	Range	Sequence	Modification
		700.3259 944.5272	2 1		5	52.9 25.2	545–556 574–583	K.TVMENFVAFVDK.C K.LVASTQAALA	
			m/z Meas	z	Score	Range	Sequence		
Albumin gil229552		66.1	561.2794	2	58.0	562–571	K.EACFAVEGPK.L		Propionamide: 3
Similar to peptidylprolyl isomerase A (cyclophilin A) gil28189246	ophilin A) gil28189246	16.4	528.2706	2		6–14	R.VSFELFADQ.V		
			806.8845	2	56.1	42–55	R.IIPGFMCQGGDFTR.H	I	Propionamide: 7
			814.8796	7	65.5	42–55	R.IIPGFMCQGGDFTR.H		Oxidation: 6; Propionamide: 7
			570.7739	2	34.7	<i>LL</i> -69	K.FDDENFILK.H		
			424.7092	7	8.82	105-111	K.TEWLDGK.H		
Galectin 1 gil57164313		14.8	433.2396	7	40.0	31–38	K.SFSLNLGK.D		
			510.2449	3	41.4	39–50	K.DDNNLCLHFNPR.F		Propionamide: 6
			530.7386	2	36.2	66–75	K.DAGAWGAEQR.E		
			484.7375	7	34.9	102-109	K.LPDGYEFK.F		
			854.9124	7	102.0	114-129	R.LNLEAINYLAAGGDFK.I	FK.I	
Ribosomal protein S15a gil14165469		14.8	487.7617	2	51.6	4-12	R.MNVLADALK.S		
			495.7657	2	51.0	4-12	R.MNVLADALK.S		Oxidation: 1
			443.2301	7	33.2	37-43	R.FLTVMMK.H		Oxidation: 6
			436.2702	2	36.2	61–68	K.IVVNLTGR.L		
			564.2976	7	33.3	26-68	K. WQNNLLPSR.Q		
			743.3617	_	25.1	125-130	K.ILGFFF		
Hemoglobin subunit alpha (Alpha-globin) gill 22499	11122499	14.9	536.2557	2	56.5	31–39	R.MFLSFPTTK.T		
			544.2669	2	53.1	31–39	R.MFLSFPTTK.T		Oxidation: 1
			409.7242	7	42.3	95-98	R.VDPVNFK.L		
			640.3467	2	59.9	127-138	K.FLANVSTVLTSK.Y		
Keratin 7 gil114051856		51.5	414.2073	7	41.6	103-109	K.FASFIDK.V		
			651.8305	2	88.2	255–266	R.SLDLDSIIAEVK.A		
			639.3388	,	79.3	384–394	K.LALDIEIATYR.K		
Histone H2A (tentative) cs39 gil329663492		13.9	472.7663	7	30.7	21–29	R.AGLQFPVGR.V		
			425.7575	7	40.1	82-88	R.HLQLAIR.N		
			644.3829	ω,	30.9	100-118	K.VTIAQGGVLPNIQAVLLPK.K	7LLPK.K	
			441.2868	7	55.7	1111–118	N.IQAVLLPK.K		



Keratin 1tType II cytoskeletal partial (tentative) gil42622442253.3Hemoglobin, epsilon 1 gil1603325116.1Ribosomal protein L30 gil450663112.8Ribosomal protein L23 gil7804249214.8Chain A, the structure of crystalline profilin-beta-actin gil15788140341.6	738.3828					
16.1 12.8 14.8	570 2531	0, 0	52.8	78–89	R.FLEQQNQVLQTK.W R.DYOEI MATK I	Ovidation: 6
16.1 12.8 14.8 41.6	517.2682			362-370	R.TLLEGEESR.M	CAIMAIDII: 0
12.8	536.7701			84–93	K.GAFAKLSELH.C	
12.8 14.8	563.7706	7	27.6	97–105	K.LHVDPENFR.L	
14.8	684.3824	2	, 20.2	45–56	K.LVILANNCPALR.K	Propionamide: 8
14.8	886.4514	,	75.5	91-106	R.VCTLAIIDPGDSDIIR.S	Propionamide: 2
41.6	992.5023	,	78.7	16–35	R.ISLGLPVGAVINCADNTGAK.N	Propionamide: 13
41.6	730.3743	7	47.0	52–66	R.LPAAGVGDMVMATVK.K	
	744.3660	es es	42.7	291–311	K.DLYANTVLSGGTTMYPGIADR.M	Oxidation: 14
	581.3043	2	33.3	315–325	K.EITALAPSTMK.I	
	506.2445	8	6.44	359–371	K.QEYDESGPSIVHR.K	
Keratin 10 gil27805977 54.8	405.2173	2	26.0	138-144	R.LASYLDK.V	
	516.2800	2	55.2	239–247	R.VLDELTLTK.T	
	555.2534	2	36.6	316–324	R.DAEAWFNEK.S	
Heparin-binding protein 15—bovine gil627739	621.8374		73.5	52-64	K.AGNLGGGVVTIER.S	
	604.3319	2	41.7	62-69	K.ITVTSEVPFSK.R	
Urocortin precursor gil3600091 8.1	566.4075	_	32.3	1–5	HALLL.L	
	679.4736	_	43.6	1–6	HALLLL.L	
	792.5419	_	37.9	1-7	HALLLLL.A	
Keratin 6L (Keratin 72) Partial (tentative) gil404313481	665.3429	2	60.5	193-204	R.NLDLDSIIAEVK.A	
PREDICTED: similar to ribosomal protein S16 gil76614740	547.8477	,	71.1	51-60	K.LLEPVLLLGK.E	
	442.7557	7	29.0	117-124	R.TLLVADPR.R	
Ribosomal protein P2gil27807523	628.8390	7		50-61	K.NIEDVIAQGIGK.L	
	925.4938	ω,	29.9	62–94	K.LASVPAGGAVAVSAAPGSAAPAAGSAPAAAEEK.K	
ii in 15.5	591.2878	7	46.2	11-20	R.SSENFDELLK.A	
complex with all-trans-retinoic acid and a synthetic retinoid gil999883	547.7723	7	21.7	12-20	S.SENFDELLK.A	
	426.7193	7	20.8	99-09	R.TTEINFK.V	
Hemoglobin gamma gil229222	403.5668	es v	47.3	120-131	K.VVTGVADALAHR.Y	
	505.7632	2	39.2	122-131	V.TGVADALAHR.Y	
PREDICTED: 40S ribosomal protein S26-2-like gil119893939	827.4007	2	6.09	52-66	R.DISEASVFDAYVLPK.L	
Thioredoxin gil27806783	714.3404	2	81.2	9–21	K.YAFQEALNSAGEK.L	
Ribosomal protein S19 gil4506695	852.3796	,	79.3	44–56	K.EL.APYDENWFYTR.A	
Ribosomal protein S12 gil14277700	538.2801	7	52.2	85-93	K.LGEWVGLCK.I	Propionamide: 8
	521.7557	6	25.2	122–129	K.DVIEEYFK.C	



Propionamide: 4, Propionamide: 3, 4 Propionamide: K.FADLSEAANRNNDALR.Q R.DGQVINETSQHHDDLE.-R.LQDEIQNMKEEMAR.H K.ILLAELEQLKGQGK.S K.AADETWEPFASGK.T R.TLYTSSPGGVYATR.S R.TNEKVELQELNDR.F R.TYSLGSALRPSTSR.T R.RQVDQLTNDKAR.V K.NLQEAEEWYKSK.F K.SLHTLFGDELCK.V K.LKECCDKPVLEK.S R.QVDQLTNDKAR.V R.DTQSGSLLFIGR.L Y.TSSPGGVYATR.S K.NLQEAEEWYK.S L.KECCDKPVLEK.S R.LGDLYEEEMR.E R.IVEVFEIGPK.R K.SLSQQIENIR.S R.ADEAFEALR.I R.KLLEGEESR.I K. VLTEIIASR.T R.SYVTTSTR.T K.YLYEVAR.R K.LLEGEESR.I R.LSQKFPK.A K.STELLIR.K 1225-1234 1236-1245 101-113 130-143 159-170 160-170 394-405 283-292 283-294 46-155 295-310 451-466 218-224 108-116 365-378 102-410 403-410 137 - 143274-285 275-285 Range 81–89 37-50 51-64 54-64 58-64 29-36 92-29 Score 61.5 54.8 48.8 63.8 54.2 70.7 63.1 α 7 511.2416 499.3015 548.3016 481.9619 594.3100 416.2444 514.0132 627.8278 429.9197 508.9493 592.9988 512.9748 457.2635 478.6045 565.8224 647.3377 704.8139 457.7568 529.9741 555.3464 578.9794 530.8113 424.2777 516.3073 501.2975 736.9075 478.6056 466.7651 m/z Meas 351.0 138.9 46.5 13.2 35.9 66.3 15.7 10.2 53.7 PREDICTED: collagen, type XII, alpha 1 isoform 1 gil194669778 Serpin peptidase inhibitor, clade H (heat shock Similar to H3 histone, family 3A gil28189807 protein 47), member 1 (collagen binding Annexin V = CaBP33 isoform gil260137 Collagen, type I, alpha 1 gil77404252 protein 1) gil114051505 Fransthyretin gil27806789 Elongin B gil77736578 Vimentin gil145226795 Table 1 continued



Table 1 continued							
		m/z Meas	z	Score	Range	Sequence	
		435.9076	3		276–285	K.ECCDKPVLEK.S	Propionamide: 2, 3
		480.6397	3		336–347	R.RHPEYAVSVLLR.L	
		542.6841	3		413–427	R.KAPQVSTPTLVEISR.S	
		456.7707	2		459–465	R.LCVLHEK.T	Propionamide: 2
		518.6501	3		459–471	R.LCVLHEKTPVSEK.V	Propionamide: 2
		471.2998	4		459–474	R.LCVLHEKTPVSEKVTK.C	Propionamide: 2
		583.7956	2		475–483	K.CCTESL VNR.R	Propionamide: 1, 2
		571.8911	2		524-533	K.KQTALVELLK.H	
		507.8420	2		525-533	K.QTALVELLK.H	
		700.3930	2		545–556	K.TVMENFVAFVDK.C	
Chain a, structure of bovine beta-actin-profilin	41.6	488.7561	2		18–27	K.AGFAGDDAPR.A	
complex with actin bound atp phosphates		400.2677	3		28–38	R.AVFPSIVGRPR.H	
solvent accessible gill 3 / 8 / 8 2 1 0		514.8330	2		30–38	V.FPSIVGRPR.H	
		586.3213	2		39-49	R.HQGVMVGMGQK.D	
		452.2426	3		50-61	K.DSYVGDEAQSKR.G	
		400.7960	2		61–67	K.RGILTLK.Y	
		652.0678	3		95–112	R.VAPEEHPVLLTEAPLNPK.A	
		541.9897	3		177–190	R.LDLAGRDLTDYLMK.I	
		895.9922	2		238–253	K.SYELPDGQVITIGNER.F	
		516.9768	3		312–325	R.MQKEITALAPSTMK.I	
		581.3383	2		315–325	K.EITALAPSTMK.I	
		462.3093	2		328–335	K.IIAPPERK.Y	
Serum albumin precursor (BSA) gil1351907	69.2	729.3666	2		286–297	K.YICDNQDTISSK.L	Propionamide: 3
PREDICTED: collagen, type XII, alpha 1	351.0	594.3759	2		366–376	K.VLLIPMTTGSR.Q	
isoform 1 gil194669778		495.3179	2		544-552	K.VMILITDGK.S	
		533.7822	7		822–831	R.VSDPTTSTMK.L	
		522.6220	3		1001-1013	K.TLKVDEETENTMR.V	
		429.6184	3		1225-1235	R.IVEVFEIGPKR.V	
		465.2896	7		1806-1813	R.QNSVLLQK.L	
		529.3292	7		2352–2361	R.LKLSPADGTR.G	
		570.3764	2		2502-2512	K.ALALGALQNIR.Y	
		479.3126	2		2545–2553	K.VLVVVTDGR.S	
Hemoglobin subunit beta gil122569	16.0	475.7852	2		8–16	K.AAVTAFWGK.V	
		637.8967	7		30–39	R.LLVVYPWTQR.F	
		633.4517	7		104–115	K.LLGNVLVVVLAR.H	
		403.2622	3		132–143	K.VVTGVANALAHR.Y	
		503.3062	3		132–145	K.VVTGVANALAHRYH	



Table 1 continued

Propionamide: 4, 9 Propionamide: 7 Propionamide: 5 Propionamide: 3 Propionamide: 6 Propionamide: 5 Propionamide: 1 K.SGDRGETGPAGPAGPIGPVGAR.G K.L.SLEGDHSTPPSAYGSVK.A R.NSLCIENSCIAAHDKR.G K.TPAQYDASELKASMK.G V.GDHAAEYGAEALER.M R.LYGPSSVSFAEDFVR.S R.TPCVGDKDSSPGVR.T R.LHFFMPGFAPLTSR.G K.ARPNCGGNLLGVR.T R.CLVEKGDVAFVK.D R.NMSVIAHVDHGK.S K.GVVEVTHDLQK.H T.QVAGTPMFVVK.A R.QHGPNVCAVQK.L R.DTQSGSLLFIGR.L R.VFSGLVSTGLK.V R.SPYQLVLQHSR.L K.IGGIGTVPVGR.V N.NMMAACDPR.H K.LAVNMVPFPR.L R.SAGWNIPMGK.L R.TNQELQEINR.V R.YGTLFTMDR.M R.YLTVAAVFR.G K.SVPMVPPGIK.Y K.STTTGHLIYK.C R.YYGYTGAFR.C K.LLEACTFHKP.-R.QTVAVGVIK.A M.VNFTVDQIR.A K.LRVDPVNFK.L R.MFLSFPTTK.T R.FSALQYLR.L K.ILGPLSYSK.I R.TILMMGR.Y C.KFAELKEK.I R.VDPVNFK.L Sequence 1062-1083 549-560 775-785 134-148 309-319 394-405 470-485 488-496 136-145 540-548 595-704 314-326 131-439 416-426 150-456 143-152 105 - 119232-239 301 - 309256-266 371-378 94-100 92-100 Range 21–32 27–36 37-50 72-80 84-92 28-38 43–53 19–32 54-73 33-41 11-28 2-10 Score m/z Meas 554.3556 408.9177 615.6768 513.3349 136.5839 837.4632 479.7720 552.2933 512.8243 489.3116 196.8209 157.8068 546.3252 411.2449 588.8410 572.3558 540.9852 540.2708 520.3285 443.2714 196.9611 536.3116 544.3434 109.7446 530.7987 549.2922 160.2814 659.3755 547.3074 199.3054 466.6144 196.9362 547.3797 117.9054 110.5771 622.8461 560.8341 138.9 220.8 38.5 95.3 20.0 46.5 15.2 38.7 50.1 74.4 77.7 Serpin peptidase inhibitor, clade H (heat shock protein 47), member 1 (collagen binding protein 1) gil114051505 PREDICTED: similar to elongation factor 1 alpha gil119909776 Eukaryotic translation elongation factor 2 gil115497900 Hemoglobin subunit alpha gil110831923 Collagen, type I, alpha 1 gil77404252 LOC539596 protein gil157278885 Tubulin beta-3 gil108744053 Transferrin gil114326282 Annexin A2 gil73586982 Aggrecan gil37953323 Lumican gil27806853



Table 1 continued							
		m/z Meas	z	Score	Range	Sequence	
Similar to H3 histone, family 3A gil28189807	10.2	516.8267	2		42–50	R.YRPGTVALR.E	
		416.2701	2		58–64	K.STELLIR.K	
		445.9321	8		74–84	R.EIAQDFKTDLR.F	
Chain a, tubulin-colchicine-phomopsin a: stathmin-like	50.0	573.6727	3		216–229	R.NLDIERPTYTNLNR.L	
domain complex gil209870469		508.3180	2		327–336	K.DVNAAIATIK.T	
		460.9373	3		391–401	R.LDHKFDLMYAK.R	
Histone H4 (Partial?) gil27806945	7.6	590.8404	2		30–39	R.ISGLIYEETR.G	
		489.6403	3		64–76	K.TVTAMDVVYALKR.Q	
PREDICTED: pyruvate kinase, muscle gil194670470	57.9	687.3965	2		44–56	R.NTGIICTIGPASR.A	Propionamide: 6
		420.7901	2		448–455	R.APIIAVTR.N	
Collagen, type I, alpha 2 gil27806257	129.0	665.8729	2		979–994	E.PGPAGAVGPAGAVGPR.G	
		599.3233	2		1247–1256	K.EMATQLAFMR.L	
		531.3214	7		1356–1364	R.LNIGPVCFK	Propionamide: 7
PREDICTED: similar to tenascin N gil119908602	143.1	497.6171	3		113–124	K.KLEEEMAEVKER.C	
		538.7824	2		130–139	R.CCPGAAGLSR.H	Propionamide: 1, 2
Cartilage linking protein 1 gil27805853	40.3	500.8140	2		40-48	R.LLVEAEQAK.V	
		510.3162	2		289–297	K.VGQIFAAWK.L	
Lamin A/C (tentative) gil74354719	65.2	522.3201	2		225–233	T.RLVEIDNGK.Q	
		584.9976	3		281–296	R.NSNLVGAAHEELQQSR.I	
Chain P, the structure of crystalline profilin-beta-actin gil576369	14.9	727.9084	7		69–95	R.SSFFVNGLTLGGQK.C	
Transthyretin gil27806789	15.7	704.8664	2		26-68	K.AADETWEPFASGK.T	
PREDICTED: similar to inositol polyphosphate-4-phosphatase, type 1 isoform 2 gill 94671317	125.2	417.2756	2		695–701	S.LGIMDLR.N	Oxidation: 4
PREDICTED: similar to Chromosome 13 open reading frame 28 gil119904978	19.2	766.4805	2		2-17	M.AATTGVALLVLLLYGG.Q	



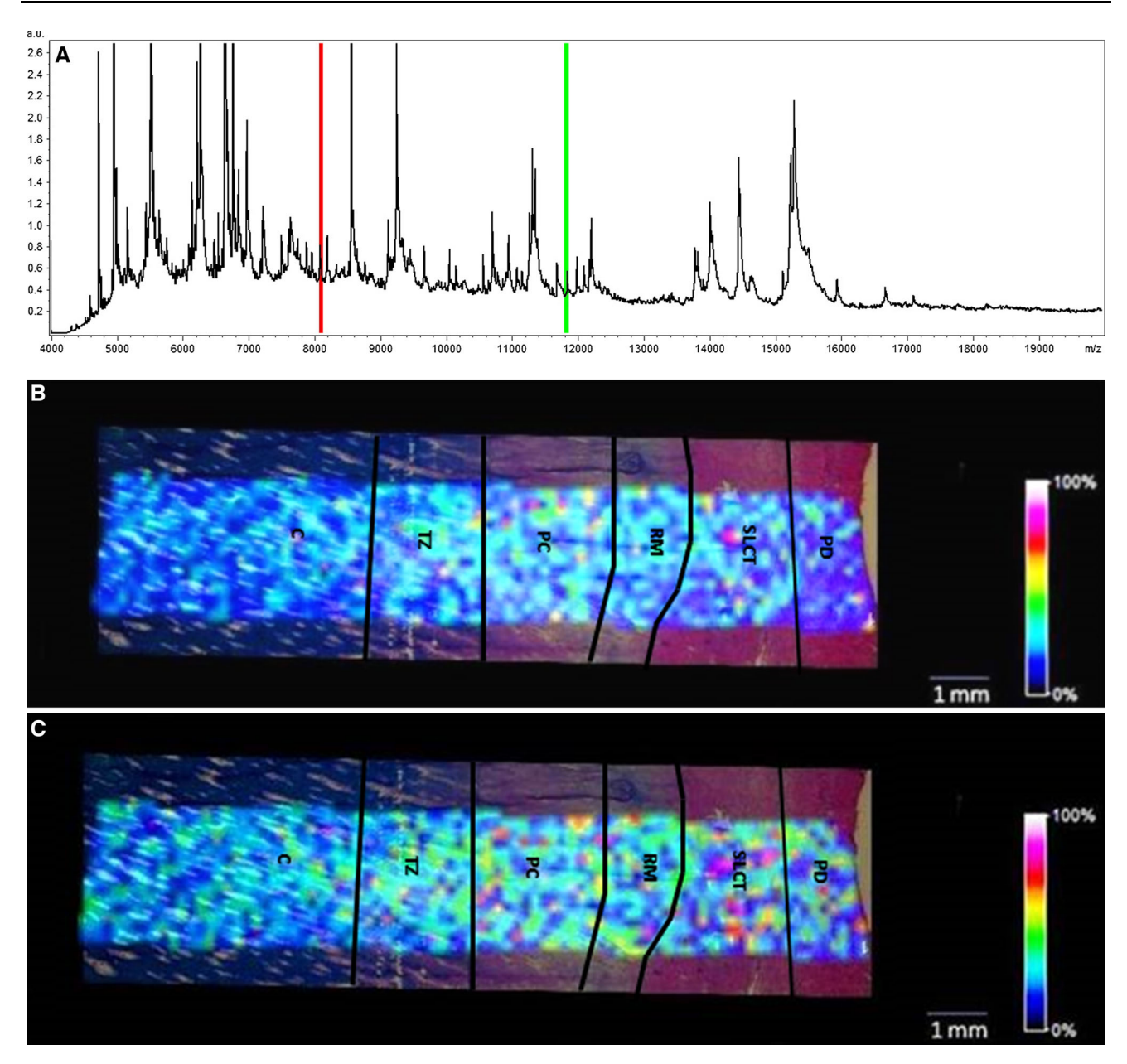


Fig. 2 Total ion count spectrum and the superimposed ion images (resolution set at 200 um) on frozen antler tip sections from the 9-month-old deer in the range between m/z 4000 and 20,000. a Total ion count spectrum showing two selected protonated ion intensities:

m/z 8100 (*red bar*) and m/z 11,800 (*green bar*). **b** Superimposed ion image for m/z 8100 (urocortin precursor). **c** Superimposed ion image for m/z 11,800 (thioredoxin). (Color figure online)

that proliferation of the blood vessels occurs in the region distal to the RM layer and proximal to the cartilage region. The expression profile of VEGF mRNA in the precartilage and transition layers would be supportive of these molecules having a role in the growth of the vascular system. No VEGF mRNA was found within the vascular layer, suggesting that other factors must drive the growth of vessels outside the precartilage zone, such as mechanical stretch [40]. It is also possible that VEGF has important direct and indirect effects on the process of chondrogenesis

and the subsequent formation of bone in antler growth, as it has been reported that VEGF has significant direct effects on mesenchymal stem cell recruitment and cartilage formation [41].

Thymosin beta-10 was previously shown to be highly expressed in the layers of the vascular, transition, and cartilage in the antler tip [42], which is consistent with the finding of the present study. Thymosin beta-10 plays an important role in the organisation of the cell structure by binding to and sequestering actin and thus modulating the



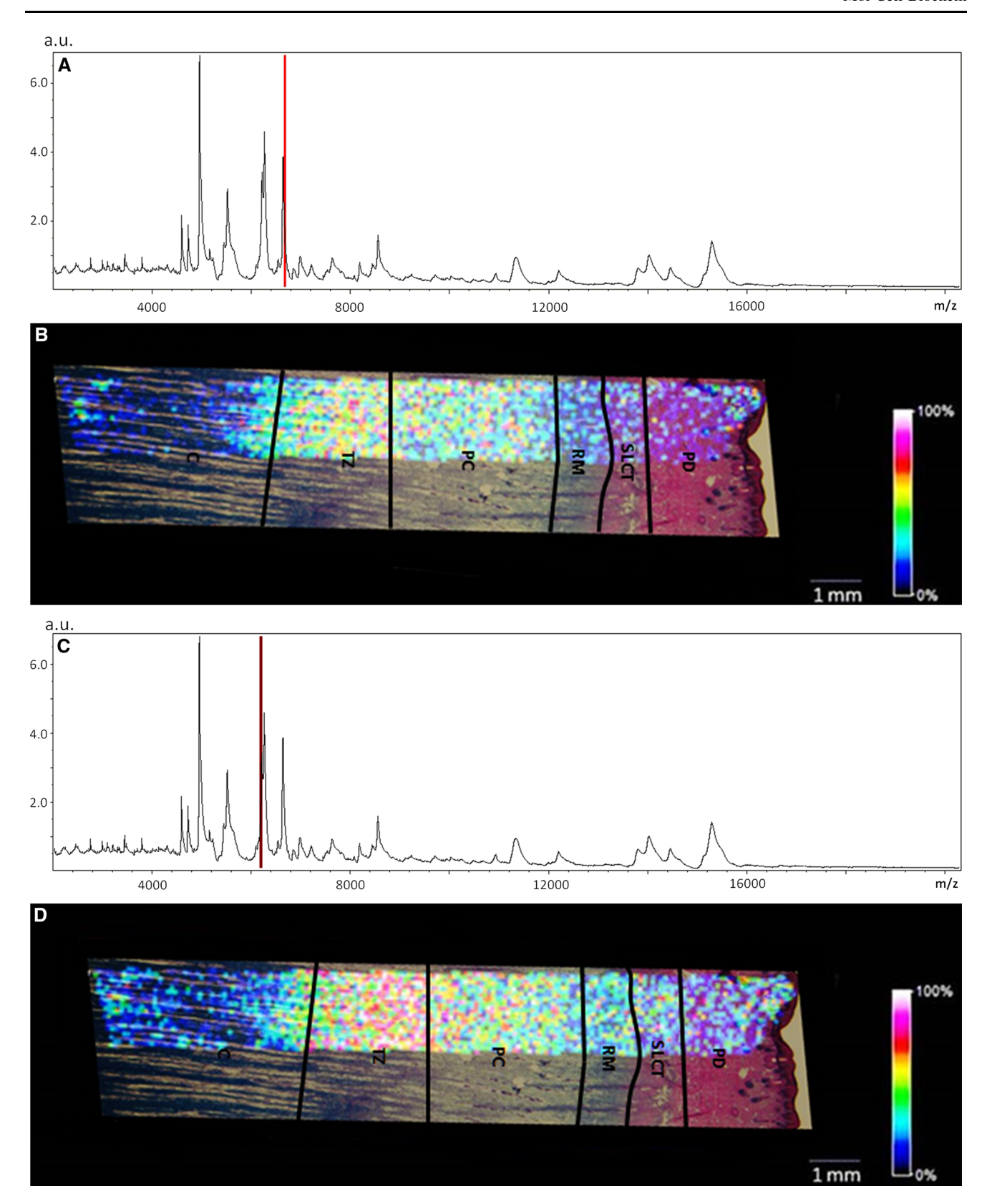


Fig. 3 Total ion count spectrum and the superimposed ion images (resolution set at 100 um) on frozen antler tip sections from a 3-year-old deer in the range between m/z 3000 and 20,000. a Total ion count spectrum, showing protonated ion intensity at m/z 6679 (red bar).

b Superimposed ion image for m/z 6679 (VEGF). **c** Total ion count spectrum showing protonated ion intensity at m/z 6200 ($brown\ bar$). **d**. Superimposed ion image for m/z 6200 (thymosin beta-10). (Color figure online)



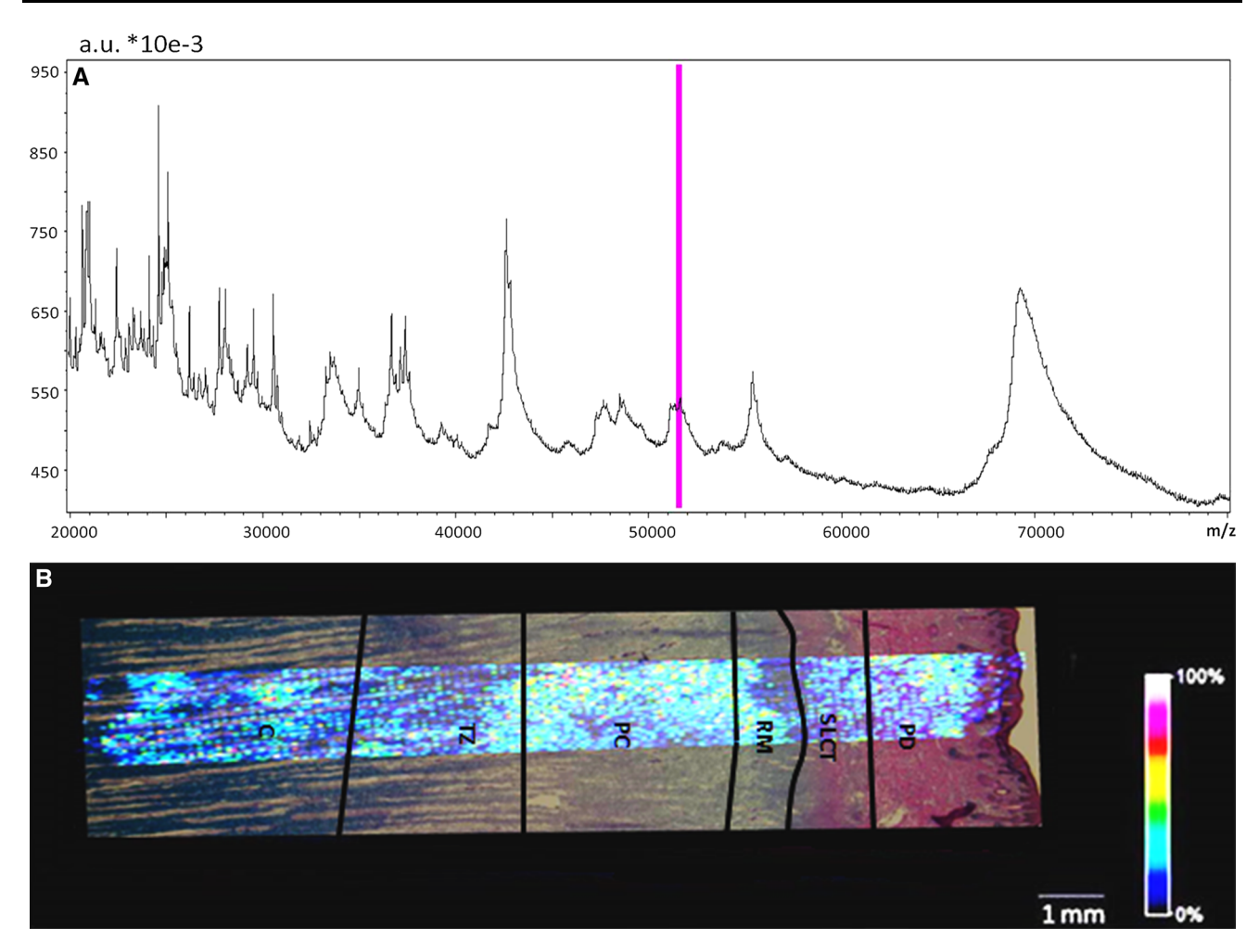


Fig. 4 Total ion count spectrum and the superimposed ion image (resolution set at 200 um) on a frozen antler tip section from the 3-year-old deer in the range between m/z 20,000–80,000. a Total ion

count spectrum showing protonated ion intensity at m/z 51,475 (*pink bar*). **b** Superimposed ion image for m/z 51,475. (Color figure online)

cytoskeleton. This rearrangement of the cytoskeleton is essential for the processes of angiogenesis and nerve development during foetal development [43]. The abundant expression of Thymosin beta-10 in vascular cells is consistent with a role in the development of blood vessels within antlers.

Extending the mass range beyond m/z 20,000

The techniques used for matrix application in the MALDI-IMS, described so far, have yielded useful signals but typically only with high intensities below m/z 20,000. A robust imaging approach should therefore be explored to increase this dynamic range as a large proportion of proteins in antler tips lies above the m/z 20,000 range [23–25]. The sandwich technique used in this study dramatically increased the signal sensitivity from proteins between m/z 20,000 and m/z 43,000 as depicted in the overall ion spectrum (Fig. 4a). As an example, the distribution of a

51.4 kDa compound is clearly discernable (Fig. 4b). This compound has a distinct distribution with the highest density in the dermis and the precartilage and the lowest density in the mesenchyme and the cartilage (Fig. 4b). Both antler dermis and precartilage are known to synthesise type I collagen [44]. Due to the nature of the distribution of this 51.4 kDa molecule, it is highly probable that it might play a role in type I collagen synthesis and secretion.

Enhancement of the signal intensity of higher molecular weight proteins was possibly due to the combination of reagents used in the sandwich technique. Previous studies have demonstrated the efficacy of Triton X-100 in solubilising hydrophobic proteins [45] and favourably influencing image quality in MALDI-IMS [32]. Although we were not able to identify these high-molecular weight proteins in the initial experiments, this technique does demonstrate the potential in enhancing ion intensity at the higher mass range, which could help understand the spatial



distribution of a larger set of proteins in future antler studies.

Technical aspects of MALDI-IMS for antler tissues

In order to properly visualise the spatial distribution of proteins across the deer antler sections using MALDI-IMS, various sample preparation techniques, each suited for the protein mass range, were trialled in this study.

Sample preparation forms a vital role in obtaining optimal ionisation of analytes to produce good quality ion images. The steps involved in preparing samples should include adequate rinsing as it is important to remove endogenous contaminants such as lipids and biological salts that can have an adverse effect on ionisation efficiency [46]. The sequential washing in graded ethanol for imaging proteins below the m/z 20,000 range, adopted in this study, provided good signal intensities, possibly due to the removal of lipids that can compete with proteins for ionisation [47]. We employed a serial wash with ethanol based on a previous study that clearly showed the efficacy of ethanol washes compared to other non-polar solvent washes [48].

Homogenous coating of the matrix is another critical factor in obtaining good ion images [49, 50]. A balance is required between the amount of wetness on the sample surface and the time of drying between matrix applications. This ensures efficient extraction of the sample compounds and mixing with the matrix solution. A homogeneous matrix coating was obtained for the deer antler samples using a vibrational vaporisation device (Bruker) in this study. This device allowed for an even distribution of matrix droplets with controlled drying time in between matrix applications for optimal extraction of analytes and matrix thickness.

In order to establish optimal methodologies for imaging experiments, the initial set of samples (for urocortin and thioredoxin) were imaged at 200 μm resolution to get a broader perspective of the functionally different regions of the deer antler tip. A lower resolution of 200 μm was also chosen for quicker scans to determine whether the sample preparation method gave satisfactory signal intensities. The 100 μm high resolution in the later experiments proved adequate for spatial correlation of ion images within antler growth centre tissue layers.

Acknowledgments The authors would like to thank Invermay deer farm crew and Otago Venison Ltd for helping collect antler tissue samples.

Author contributions C.L., S.DC., S.C., C.M., and J.D conceived and designed the experiments. S.DC., W.W., and C.L performed the experiments. S.DC., W.W., C.L., S.C, and C.M analysed the data. C.L., S.DC., S.C., C.M., W.W., and J.D wrote this paper.

Compliance with ethical standards

Conflict of interest The authors declare that they have no conflict of interest.

References

- Li C, Yang F, Sheppard A (2009) Adult stem cells and mammalian epimorphic regeneration-insights from studying annual renewal of deer antlers. Curr Stem Cell Res Ther 4(3):237–251
- Goss RJ (1983) Deer antlers. Regeneration, function and evolution. Academic Press, New York
- Kierdorf U, Li C, Price JS (2009) Improbable appendages: deer antler renewal as a unique case of mammalian regeneration. Semin Cell Dev Biol 20(5):535–542
- 4. Li C, Zhao S, Wang W (1988) Biology of deer antler. Chinese Press of Agricultural Sciences, Beijing
- Goss RJ (1970) Problems of antlerogenesis. Clin Orthop 69:227–238
- Li C (2003) Development of deer antler model for biomedical research. Adv Res Updat 4(2):256–274
- Kierdorf UK, Kierdorf H (2011) Deer antlers—a model of mammalian appendage regeneration: an extensive review. Gerontology 57(1):53–65
- Chapman DI (1975) Antlers-bones of contention. Mammal Rev 5(4):121–172
- Banks WJ, Newbrey JW (1982) Light microscopic studies of the ossification process in developing antlers. In: Brown RD (ed) Antler Development in Cervidae. Caesar Kleberg Wildl. Res. Inst., Kingsville
- Goss R (1983) Chondrogenesis in regenerating systems. In: Hall B (ed) Cartilage: biomedical aspects, vol 3. Academic Press, New York, pp 267–370
- Kierdorf H, Kierdorf U, Szuwart T, Gath U, Clemen G (1994) Light microscopic observations on the ossification process in the early developing pedicle of fallow deer (Dama dama). Anat Anz 176(3):243–249
- Li C, Suttie JM (1994) Light microscopic studies of pedicle and early first antler development in red deer (*Cervus elaphus*). Anat Rec 239(2):198–215
- Li C, Suttie JM (1998) Electron microscopic studies of antlerogenic cells from five developmental stages during pedicle and early antler formation in red deer (*Cervus elaphus*). Anat Rec 252(4):587–599
- Li C, Clark DE, Lord EA, Stanton JA, Suttie JM (2002) Sampling technique to discriminate the different tissue layers of growing antler tips for gene discovery. Anat Rec 268(2):125–130
- Colitti MA, Allen SP, Price JS (2005) Programmed cell death in the regenerating deer antler. J Anat 207(4):339–351. doi:10.1111/ j.1469-7580.2005.00464.x
- Li C, Suttie JM (2003) Tissue collection methods for antler research. Eur J Morphol 41(1):23–30
- 17. Gyurjan I Jr, Molnar A, Borsy A, Steger V, Hackler L Jr, Zomborszky Z, Papp P, Duda E, Deak F, Lakatos P, Puskas LG, Orosz L (2007) Gene expression dynamics in deer antler: mesenchymal differentiation toward chondrogenesis. Mol Genet Genomics 277(3):221–235. doi:10.1007/s00438-006-0190-0
- Molnar A, Gyurjan I, Korpos E, Borsy A, Steger V, Buzas Z, Kiss I, Zomborszky Z, Papp P, Deak F, Orosz L (2007) Identification of differentially expressed genes in the developing antler of red deer *Cervus elaphus*. Mol Genet Genomics 277(3):237–248. doi:10.1007/s00438-006-0193-x



- Villanyi Z, Gyurjan I, Steger V, Orosz L (2008) Plaque-based competitive hybridization. J Biomol Screen 13(1):80–84. doi:10. 1177/1087057107310876
- Yao B, Zhao Y, Zhang H, Zhang M, Liu M, Liu H, Li J (2012) Sequencing and de novo analysis of the Chinese Sika deer antlertip transcriptome during the ossification stage using Illumina RNA-Seq technology. Biotechnol Lett 34(5):813–822. doi:10. 1007/s10529-011-0841-z
- Borsy A, Podani J, Steger V, Balla B, Horvath A, Kosa JP, Gyurjan I Jr, Molnar A, Szabolcsi Z, Szabo L, Jako E, Zomborszky Z, Nagy J, Semsey S, Vellai T, Lakatos P, Orosz L (2009) Identifying novel genes involved in both deer physiological and human pathological osteoporosis. Mol Genet Genomics 281(3):301–313. doi:10.1007/s00438-008-0413-7
- Pita-Thomas W, Nieto-Sampedro M, Maza RM, Nieto-Diaz M (2010) Factors promoting neurite outgrowth during deer antler regeneration. J Neurosci Res 88(14):3034–3047. doi:10.1002/jnr. 22459
- Li C, Harper A, Puddick J, Wang W, McMahon C (2012) Proteomes and signalling pathways of antler stem cells. PLoS One 7(1):e30026. doi:10.1371/journal.pone.0030026
- Park HJ, do Lee H, Park SG, Lee SC, Cho S, Kim JJ, Bae H, Park BC (2004) Proteome analysis of red deer antlers. Proteomics 4(11):3642–3653
- Sui Z, Yuan H, Liang Z, Zhao Q, Wua Q, Xia S, Zhang L, Huo Y, Zhang Y (2013) An activity-maintaining sequential protein extraction method for bioactive assay and proteome analysis of velvet antlers. Talanta 107:189–194. doi:10.1016/j.talanta.2013. 01.015
- Mark L, Maasz G (2012) Pirger Z (2012), High resolution spatial distribution of neuropeptides by MALDI imaging mass spectrometry in the terrestrial snail, Helix pomatia. Acta Biol Hung 2:113–122. doi:10.1556/ABiol.3.2012.Suppl.2.15
- Lay JO Jr, Gidden J, Liyanage R, Emerson B, Durham B (2012)
 Rapid characterization of lipids by MALDI MS. Part 2: artifacts, ion suppression, and TLC MALDI imaging. Lipid Technol 24(2):36–40. doi:10.1002/lite.201200174
- Dani FR, Francese S, Mastrobuoni G, Felicioli A, Caputo B, Simard F, Pieraccini G, Moneti G, Coluzzi M, Della TA, Turillazzi S (2008) Exploring proteins in Anopheles gambiae male and female antennae through MALDI mass spectrometry profiling. PLoS One. doi:10.1371/journal.pone.0002822
- Chaurand P, Fouchecourt S, DaGue BB, Xu BJ, Reyzer ML, Orgebin-Crist MC, Caprioli RM (2003) Profiling and imaging proteins in the mouse epididymis by imaging mass spectrometry. Proteomics 3(11):2221–2239. doi:10.1002/pmic.200300474
- Balluff B, Schone C, Höfler H, Walch A (2011) MALDI imaging mass spectrometry for direct tissue analysis: technological advancements and recent applications. Histochem Cell Biol 136(3):227–244. doi:10.1007/s00418-011-0843-x
- Schwartz SA, Reyzer ML, Caprioli RM (2003) Direct tissue analysis using matrix-assisted laser desorption/ionization mass spectrometry: practical aspects of sample preparation. J Mass Spectrom 38(7):699–708. doi:10.1002/jms.505
- Leinweber BD, Tsaprailis G, Monks TJ, Lau SS (2009) Improved MALDI-TOF imaging yields increased protein signals at high molecular mass. J Am Soc Mass Spec 20(1):89–95. doi:10.1016/ j.jasms.2008.09.008
- Davidson SM, Yellon DM (2009) Urocortin: a protective peptide that targets both the myocardium and vasculature. Pharmacol Rep 61(1):172–182
- 34. Venkatasubramanian S, Newby DE, Lang NN (2010) Urocortins in heart failure. Biochem Pharmacol 80(3):289–296. doi:10.1016/j.bcp.2010.03.032

- 35. Bale TL, Lee KF, Vale WW (2002) The role of corticotropinreleasing factor receptors in stress and anxiety. Integr Comp Biol 42(3):552–555. doi:10.1093/icb/42.3.552
- Clark DE, Lord EA, Suttie JM (2006) Expression of VEGF and pleiotrophin in deer antler. Anat Rec A Discov Mol Cell Evol Biol 288(12):1281–1293
- Lee S, Kim SM, Lee RT (2013) Thioredoxin and thioredoxin target proteins: from molecular mechanisms to functional significance. Antioxid Redox Signal 18(10):1165–1207. doi:10.1089/ars.2011.4322
- Carmeliet P, Mackman N, Moons L, Luther T, Gressens P, Van Vlaenderen I, Demunck H, Kasper M, Breier G, Evrard P, Muller M, Risau W, Edgington T, Collen D (1996) Role of tissue factor in embryonic blood vessel development. Nature 383(6595):73–75. doi:10.1038/383073a0
- Ferrara N, Bunting S (1996) Vascular endothelial growth factor, a specific regulator of angiogenesis. Curr Opin Nephrol Hypertens 5(1):35–44
- Li C (2012) Deer antler regeneration: a stem cell-based epimorphic process. Birth Defects Res Part C 96(1):51–62. doi:10.1002/bdrc.21000
- Peng H, Wright V, Usas A, Gearhart B, Shen HC, Cummins J, Huard J (2002) Synergistic enhancement of bone formation and healing by stem cell-expressed VEGF and bone morphogenetic protein-4. J Clin Invest 110(6):751–759. doi:10.1172/JCI15153
- 42. Lord E, Clark D, Martin S, Pedersen G, Gray J, Li C (2005) Suttie J Profiling genes expressed in the regenerating tip of red deer (*Cervus elaphus*) antler. In: Suttie J, Haines S, Li C (eds) Proceedings of the 2nd International Symposium on Antler Science and Product Technology. Queenstown, New Zealand, pp 129–134
- Carpintero P, Franco del Amo F, Anadon R, Gomez-Marquez J (1996) Thymosin beta10 mRNA expression during early postimplantation mouse development. FEBS Lett 394(1):103–106
- 44. Price JS, Oyajobi BO, Nalin AM, Frazer A, Russell RG, Sandell LJ (1996) Chondrogenesis in the regenerating antler tip in red deer: expression of collagen types I, IIA, IIB, and X demonstrated by in situ nucleic acid hybridization and immunocytochemistry. Dev Dyn 205:332–347
- Börnsen KO, Gass MA, Bruin GJ, von Adrichem JH, Biro MC, Kresbach GM, Ehrat M (1997) Influence of solvents and detergents on matrix-assisted laser desorption/Ionization mass spectrometry measurements of proteins and oligonucleotides. Rap Comm Mass Spec 11(6):603–609
- 46. Seeley EH, Caprioli RM (2012) 3D imaging by mass spectrometry: a new frontier. Anal Chem 84(5):2105–2110
- Aerni HR, Cornett DS, Caprioli RM (2006) Automated acoustic matrix deposition for MALDI sample preparation. Anal Chem 78(3):827-834
- Seeley EH, Oppenheimer SR, Mi D, Chaurand P, Caprioli RM (2008) Enhancement of protein sensitivity for MALDI imaging mass spectrometry after chemical treatment of tissue sections.
 J Am Soc Mass Spec 19(8):1069–1077. doi:10.1016/j.jasms. 2008.03.016
- Chaurand P, Norris JL, Cornett DS, Mobley JA, Caprioli RM (2006) New developments in profiling and imaging of proteins from tissue sections by MALDI mass spectrometry. J Proteome Res 5(11):2889–2900
- Benabdellah F, Seyer A, Quinton L, Touboul D, Brunelle A, Laprévote O (2010) Mass spectrometry imaging of rat brain sections: nanomolar sensitivity with MALDI versus nanometer resolution by TOF–SIMS. Anal Bioanal Chem 396(1):151–162. doi:10.1007/s00216-009-3031-2

